LETTER

doi:10.1038/nature23008

Pre-oral gut contributes to facial structures in non-teleost fishes

Martin Minarik[1], Jan Stundl[1,2], Peter Fabian[1], David Jandzik[1,3], Brian D. Metscher[4], Martin Psenicka[5], David Gela[5], Adriana Osorio-Pérez[6], Lenin Arias-Rodriguez[6], Ivan Horácek[1] & Robert Cerny[1]

Despite the wide variety of adaptive modifications in the oral and facial regions of vertebrates, their early oropharyngeal development is considered strictly uniform. It involves sequential formation of the mouth and pharyngeal pouches, with ectoderm outlining the outer surface and endoderm the inner surface, as a rule[1,2]. At the extreme anterior domain of vertebrate embryos, the ectoderm and endoderm directly juxtapose and initial development of this earliest ecto–endoderm interface, the primary mouth[3], typically involves ectodermal stomodeal invagination that limits the anterior expansion of the foregut endoderm[3,4]. Here we present evidence that in embryos of extant non-teleost fishes, oral (stomodeal) formation is preceded by the development of prominent pre-oral gut diverticula (POGD) between the forebrain and roof of the forming mouth. Micro-computed tomography (micro-CT) imaging of bichir, sturgeon and gar embryos revealed that foregut outpocketing at the pre-oral domain begins even before the sequential formation of pharyngeal pouches. The presence of foregut-derived cells in the front of the mouth was further confirmed by *in vivo* experiments that allowed specific tracing of the early endodermal lining. We show that POGD in sturgeons contribute to the orofacial surface of their larvae, comprising oral teeth, lips, and sensory barbels. To our knowledge, this is the first thorough evidence for endodermal origin of external craniofacial structures in any vertebrate. In bichir and gar embryos, POGD form prominent cranial adhesive organs that are characteristic of the ancient bauplan of free-living chordate larvae. POGD hence seem arguably to be ancestral for all ray-finned fishes, and their topology, pharyngeal-like morphogenesis and gene expression suggest that they are evolutionarily related to the foregut-derived diverticula of early chordate and hemichordate embryos. The formation of POGD might thus represent an ancestral developmental module with deep deuterostome origins.

In vertebrate embryos, the ectoderm gives rise to the skin, nervous system, and neural crest derivatives, whereas the endoderm is confined to the inner epithelial lining of the alimentary tract and its derived organs. In the vertebrate head, embryonic interactions between the ectoderm and endoderm occur within strictly defined locations: the primary mouth and pharyngeal slits[1,2]. Early oropharyngeal development is considered uniform and is orchestrated around pharyngeal pouching of the primitive gut cavity[5,6]. The sequential formation of pharyngeal pouches maintains separate populations of craniofacial mesenchyme, and the pharyngeal endoderm is also a prominent source of signalling molecules that pattern the development of the craniofacial skeleton[6–8]. The segmental organization of the pharynx thus represents a fundamental part of the metameric organization of the vertebrate

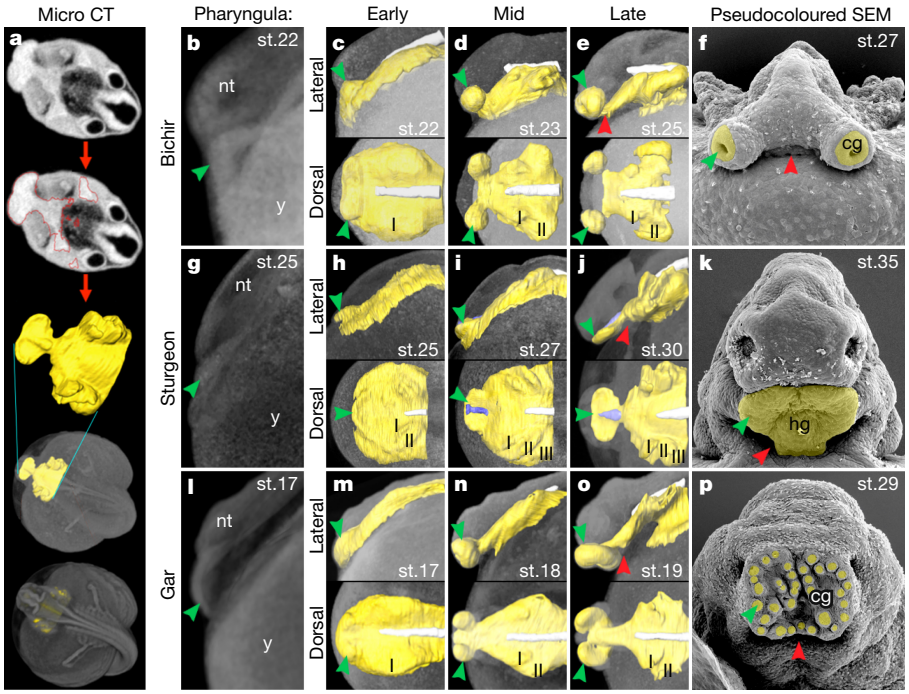

Figure 1 | Micro-CT visualization of pharyngeal development in bichir, sturgeon and gar reveals prominent POGD. a, Micro-CT technique and 3D rendered visualization of pharyngeal endoderm (yellow) within an embryo. **b**, **g**, **l**, Wholemount view of early pharyngulae of bichir (**b**), sturgeon (**g**) and gar (**l**), head to the left, showing the anterior extent of the foregut endoderm (green arrowhead). **c**–**e**, **h**–**j**, **m**–**o**, 3D models of pharyngeal development in bichir (**c**–**e**), sturgeon (**h**–**j**) and gar (**m**–**o**); endoderm yellow, POGD marked by green arrowhead, mouth marked by red arrowhead, notochord white, adenohypophysis blue, roman numerals refer to pharyngeal pouches. **f**, **k**, **p**, SEM images of bichir (**f**), sturgeon (**k**) and gar (**p**) at stages just after hatching; anteroventral views mapping micro-CT data (pseudocoloured yellow). cg, cement gland; hg, hatching gland; nt, neural tube; st, embryonic stage; y, yolk.

[1]Department of Zoology, Charles University, Prague, Czech Republic. [2]Department of Zoology, National Museum, Prague, Czech Republic. [3]Department of Zoology, Comenius University, Bratislava, Slovakia. [4]Department of Theoretical Biology, University of Vienna, Vienna, Austria. [5]University of South Bohemia in České Budějovice, Faculty of Fisheries and Protection of Waters, Research Institute of Fish Culture and Hydrobiology, South Bohemian Research Center of Aquaculture and Biodiversity of Hydrocenoses, Vodňany, Czech Republic. [6]Universidad Juárez Autónoma de Tabasco, División Académica de Ciencias Biológicas, Villahermosa, Mexico.

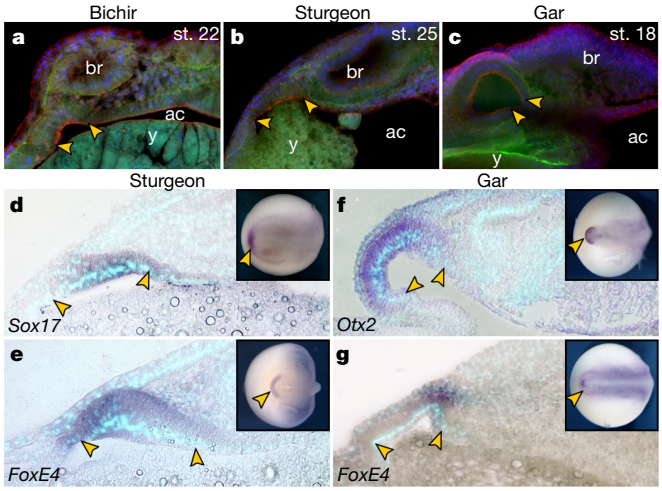

Figure 2 | Pharyngeal outpocketing in the pre-oral region, and gene expression patterns in forming POGD in bichir, sturgeon and gar embryos. a–g, Early pharyngulae of bichir (**a**), sturgeon (**b**, **d**, **e**) and gar (**c**, **f**, **g**); parasagittal sections, head to the left. **a–c**, Foregut outpocketing with POGD (yellow arrowheads). DAPI (blue) stains cell nuclei; fibronectin (green) marks cell and tissue borders; actin staining (red) indicates that apical constriction is involved in the process of POGD formation. **d–g**, *Sox17*, *FoxE4* and *Otx2* expression in forming POGD (yellow arrowheads; see Methods for details of probes). Insets show wholemounts; main images show parasagittal sections, head to the left; DAPI (blue) stains cell nuclei. ac, archenteron cavity; br, brain.

head and face[7,9]. This programme has deep deuterostome origins[10], as an expanding pharynx with mucus secretion presents the foremost morphological innovation of early deuterostomes[11].

In the vertebrate pharynx, each pair of laterally expanding pouches is contacted by corresponding ectodermal clefts, and they subsequently fuse to form pharyngeal opening slits[1,2,5]. The rostral expansion of the primitive gut is typically limited by a stomodeal invagination of the oral ectoderm, by which the ecto–endoderm contact zone is established deep inside the prospective mouth[3,4]. However, it has been suggested[12] that an early outpocketing of the primitive gut precedes mouth formation in the ancient fish bichir (*Polypterus*), shifting the anteriormost portion of the endoderm in front of the stomodeum. Paired endodermal diverticula later open to the exterior as mucus-producing adhesive organs[12]. These so-called cement glands of bichir embryos would not only represent a contribution of foregut-derived cells to the craniofacial surface, but also an additional ectoderm–endoderm orofacial interface.

Here we present detailed series of cranial endoderm development in the Senegal bichir (*Polypterus senegalus*), the European sturgeon (*Acipenser ruthenus*) and the tropical gar (*Atractosteus tropicus*) to provide new insights into this developmental process, which has remained unresolved for more than a century. These three taxa represent early-branching (non-teleost) lineages of ray-finned (actinopterygian) fishes, but share many characters with the lobe-finned (sarcopterygian) fishes, resulting in a unique mixture of ancestral and derived traits[13]. The relatively large size of bichir, sturgeon, and gar eggs makes their embryos ideal models for visualizing pharyngeal development using micro-CT imaging (Extended Data Figs 1–3). The presence of yolk granules within the endoderm allowed us to introduce high

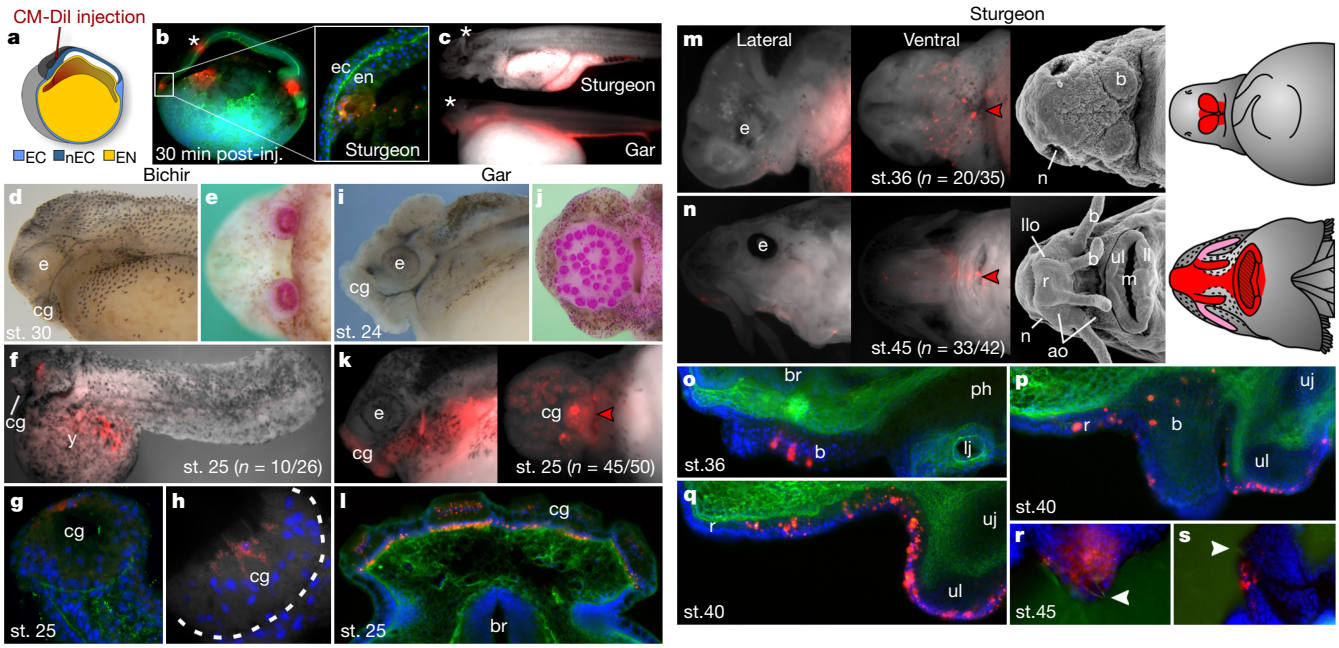

Figure 3 | Fate-mapping of the primitive gut in bichir, sturgeon and gar embryos reveals endodermal contribution to the orofacial surface. **a**, CM-DiI fate-mapping. **b**, Median section of sturgeon neurula. Asterisk shows injection site and enlarged inset shows incorporation of CM-DiI (red) into the endoderm internal to the basal lamina (fibronectin, green) at the anteriormost pole. DAPI (blue) stains cell nuclei. **c**, Experimental sturgeon and gar larvae with CM-DiI-filled gut cavities. **d**, **e**, Bichir larvae with cement glands visualized by anti-tubulin staining (**d**) (lateral view), and by mucus secretion (**e**) (ventral view; pink, PAS staining). **f**, Experimental bichir embryo with CM-DiI in pharynx and cement glands. **g**, **h**, Horizontal sections showing CM-DiI in the secretory layer of cement glands. DAPI (blue) stains cell nuclei; fibronectin (green) marks cell and tissue borders. **i**, **j**, Gar larvae with cement glands visualized by anti-tubulin staining (**i**) (lateral view), and by mucus secretion (**j**) (ventral view; pink, PAS staining). **k**, Experimental gar embryos. Wholemount lateral (left) and ventral (right) views with CM-DiI in pharynx and cement glands. Red arrowhead indicates mouth. **l**, Horizontal section showing anterior head with CM-DiI in cement glands. DAPI (blue) stains cell nuclei; fibronectin (green) marks cell and tissue borders. **m**, **n**, Experimental sturgeon embryos showing the extent of CM-DiI at stages just before (**m**) and after (**n**) mouth (red arrowhead) opens. Left to right show lateral views, ventral views, SEM images and schematics. **o–s**, Parasagittal sections, head to the left, showing contribution of the foregut endoderm (CM-DiI) in rostrum (r), barbels (b), upper lip (ul), and teeth (white arrowhead) on the upper (**r**) and lower (**s**) jaws. DAPI (blue) stains cell nuclei; fibronectin (green) marks cell and tissue borders. EC, ectoderm; nEC, neural ectoderm; EN, endoderm; e, eye; ph, pharynx; uj, upper jaw; lj, lower jaw; ll, lower lip; m, mouth; n, nostril; llo, lateral line organs.

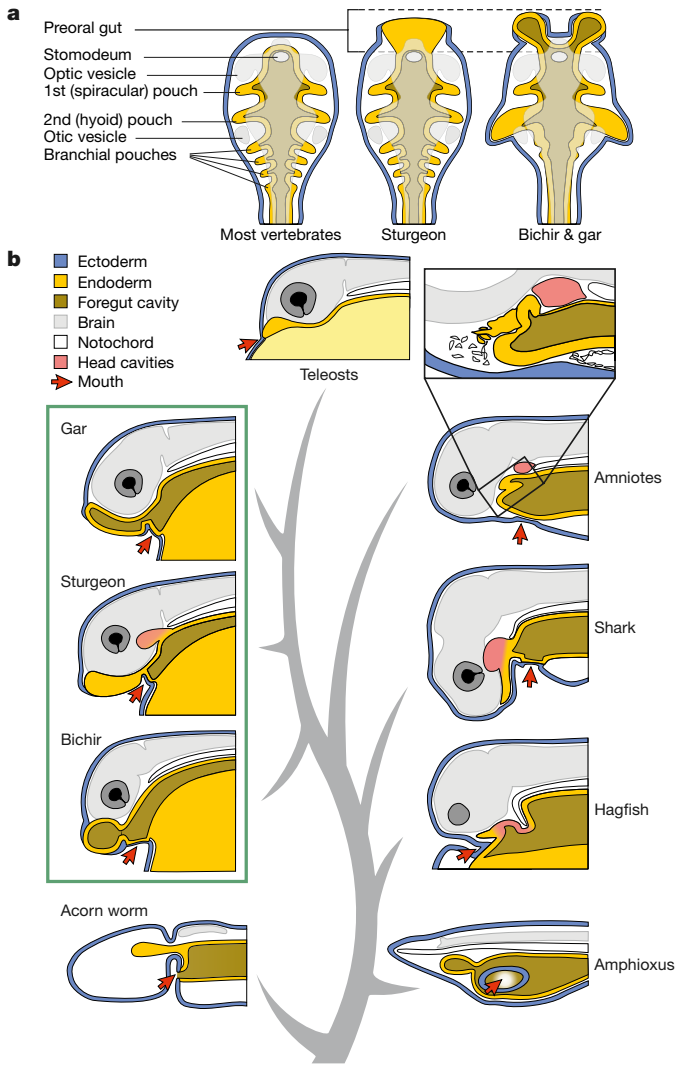

Figure 4 | Oropharyngeal development comprising POGD, and distribution of POGD on chordate phylogenetic tree. a, A common scheme of vertebrate pharynx (left) with typical pharyngeal pouches in post-oral position; the ectoderm is outside (blue), and endoderm inside (yellow). In non-teleost fishes, outpocketing of the primitive gut cavity forms prominent POGD (either single as in sturgeon, or paired as in bichir and gar) that penetrate the epidermis, and develop by morphogenesis similar to pharyngeal pouch formation. Endodermal epithelium is yellow, cavity of the primitive gut is brown, brain structures are grey. **b**, Simplified phylogenetic scheme of chordates, with the presence of POGD in hemichordates (stomochord in acorn worms[24]), cephalochordates (Hatschek's diverticula of amphioxus[31]), and in non-teleost fishes (framed). POGD seem to be reduced in teleosts[24] and can be observed as rudimentary in hagfishes[27], sharks[25] and amniotes[7,26] in the form of Seessel's pouch[28]. The top right (framed) scheme has been redrawn from ref. 26.

differential contrast (Fig. 1a) and to design 3D models of the pharyngeal development of the embryos (Fig. 1 and Extended Data Fig. 4). The earliest signs of pharyngeal differentiation occur at the cranial end of embryos (Fig. 1b, g, l), where the ectoderm and endoderm are directly juxtaposed (Fig. 1c, h, m). The most conspicuous pharyngeal outpocketing appears at the extreme anterior, below the forebrain, and it extends further cranially as the sequential formation of more caudal pharyngeal pouches proceeds (Fig. 1d, i, n). In bichirs and gars, this foregut outpocketing forms conspicuous paired club-shaped projections (Fig. 1e, o) that develop into cranial adhesive organs, prominent craniofacial structures of the free-living embryos (Fig. 1f, p). In sturgeons, the foregut initially forms a central pocket (Fig. 1h) that later extends as a shovel-like projection with a narrow part connecting it to the pharynx (Fig. 1i, j). Surrounding the forebrain ventrally (Fig. 1j), this foregut projection seemingly prefigures the entire ventral rostrum of sturgeon, including the embryonic hatching gland (Fig. 1k). Importantly, in all bichir, sturgeon, and gar pharyngula embryos, these anteriormost pouches are located in the pre-oral domain, as the prospective mouth forms posteroventrally (Fig. 1e, f, j, k, o, p). We thus name these pouches pre-oral gut diverticula (POGD).

POGD represent a true continuation of the pharyngeal cavity (Fig. 2) and develop by outpocketing of polarized epithelia, a mechanism typical of pharyngeal morphogenesis[14] (Fig. 2a–c and Extended Data Fig. 5). POGD directly contact the extreme anterior ectoderm and are situated far ahead of the notochord and prechordal mesenchyme that in sturgeon embryos later forms prominent head cavities (Extended Data Fig. 6). The endodermal identity of POGD is also consistent with the expression of the general endoderm marker *Sox17*[15] (Fig. 2), and the expression pattern of FoxE4 genes (Fig. 2 and Extended Data Fig. 7) that are typically expressed in epithelial structures separating from the pharynx[16].

To confirm the germ-layer identity of POGD, we performed *in vivo* experiments on living bichir, sturgeon and gar embryos (Fig. 3). We have designed a fate-mapping approach that allowed us to specifically mark the endodermal cells during neurulation, and to trace them until the orofacial structures became fully developed. The fluorescent cell tracker dye CM-DiI was injected into the lumen of the primitive gut through the still open cranial neural tube (Fig. 3a). The dye passes freely into the adjacent endodermal lining, forming cell membrane-impermeant products that cannot stain the ectoderm situated across the basal lamina (Fig. 3b). Consequently, in experimental bichir and gar embryos, CM-DiI-stained foregut cells were common in the internal gut derivatives and yolk cells, but also in the cranial adhesive organs of both bichir ($n = 10$ of 26) and gar ($n = 155$ of 167) (Fig. 3f, k and Extended Data Fig. 8). Within the adhesive organs, the staining was located in the outer epidermal layer (Fig. 3g, h, l), corroborating previous visualizations[12] (Fig. 1f, p). Endoderm-derived adhesive organs of bichir and gar embryos occupy major parts of their craniofacial surface (Figs 1f, p and 3e, j), and are typically innervated by the maxillary branch of the trigeminal nerve (Fig. 3d, i). They also express *Otx2*, *Otx5* and *Pitx2*[17] (Extended Data Fig. 7), as is characteristic of ectoderm-derived adhesive organs of teleost larvae and frog and ascidian tadpoles[18,19]. The disparate germ-layer origins of cranial adhesive organs might indicate independent, parallel evolution of these otherwise similar larval traits[18], or present an extreme example of developmental system drift[20] across the ectoderm–endoderm interface.

In experimental sturgeon embryos, before the mouth opened, the CM-DiI foregut cells were observed rostral to the prospective mouth and below the forebrain (Fig. 3m), confirming our micro-CT observations (Fig. 1k). During later craniofacial development, the CM-DiI signal was detected in major parts of the ventral head, including extra-oral and pre-oral positions ($n = 79$ of 117) (Extended Data Fig. 9a–d). According to our fate-mapping, the foregut-derived midline craniofacial zone covers the growing rostrum with sensory barbels (Fig. 3n). However, whereas the medial pair of barbels was commonly stained, the lateral pair was stained only rarely ($n = 7$ of 58) (Fig. 3n and Extended Data Fig. 9b–d). The apparently endoderm-derived rostrum of sturgeons (Extended Data Fig. 9e–j) is demarcated by sensory domains colonized by ampullary organs and lateral line neuromasts (Extended Data Fig. 10). To confirm the epithelial localization of the foregut-derived cells, we further analysed sections of experimental sturgeons counterstained with antibodies that visualize basal laminae. The CM-DiI signal was identified within orofacial surface epithelia, including sensory barbels (Fig. 3o, p), growing rostrum (Fig. 3p, q), and oral lips and teeth on both the upper and lower jaws (Fig. 3r, s). This is intriguing because the orofacial epithelia are typically ectodermal, and until now, a small-scale endodermal contribution to oral teeth, and some extra-oral structures such as lips, had been demonstrated only in axolotls[21]. In bichirs, sturgeons and gars, however, endoderm forms substantial parts of the orofacial epithelia (Fig. 3), as a direct result of embryonic outpocketing of the primitive gut (Fig. 4a).

The shared presence of POGD in bichirs, sturgeons and gars, the three non-teleost fish lineages, implies that this is an ancestral feature of all ray-finned fishes (Fig. 4b). In teleosts, the most derived group of ray-finned fishes, this morphogenesis seems to be suppressed owing to the radical transformation of their early development, accompanied by the loss of the primitive gut cavity[22]. However, early teleost embryos often possess hatching glands that express *FoxE4* genes, similar to sturgeon hatching glands (Fig. 2e), and that also occupy a seemingly pre-oral position[23].

POGD similar to those of bichir, sturgeon and gar embryos seem to be present in hemichordates (acorn worms), where an anterior outgrowth of the pharyngeal endoderm with a continuous gut lumen forms the stomochord[11,24]. This early pharyngeal diverticulum is characterized by *FoxE* expression[24], as it is in non-teleost fishes (Fig. 2e, g). Moreover, in amphioxus, a basal chordate, the club-shaped gland that pinches off from the pharyngeal endoderm in a pre-oral position shares high levels of *FoxE* expression with the hemichordate stomochord and with the endostyle of ascidians (a sister group of vertebrates)[16,24]. All these structures of deuterostome embryos show clear evolutionary relatedness to organs deriving from the anteriormost pharynx[24], but similar diverticula have not been fully appreciated in vertebrates before now, to our knowledge.

In most vertebrate embryos, the roof of the foregut is commonly recognized as the so-called prechordal plate, forming the cranial-most, undifferentiated mesendodermal layer[7,25,26]. However, the rostral-most part of this plate has classically been described to form rudimentary endodermal protrusions beneath the forebrain, either medial, as in shark embryos[25], or paired bilateral, as in hagfish embryos[27] (Fig. 4b). Vestigial POGD also exist in chick embryos in the form of Seessel's pouch. This was first described as a small embryonic diverticulum of the anterior gut wall[28], which forms a clear epithelial pit-like structure anteriorly abutting the prechordal mesenchyme[7,26] (Fig. 4b). All these cranial endodermal protrusions share their position in the pre-oral domain, disappear very early, before the mouth develops[7,25–27], and could be considered vestigial POGD. The formation of POGD seems highly reduced in the yolk-rich embryos of sharks, amniotes and teleost fishes, all of which independently evolved derived meroblastic cleavage with constraining effects on early endoderm formation and patterning[22,29]. As the holoblastic development of non-teleost fishes is considered ancestral for all vertebrates[30], their early development is likely to preserve conserved ancestral patterns of vertebrate embryogenesis. Thus, the formation of POGD could represent an ancient blueprint of deuterostome pharyngeal development integrated into head formation in early stages of vertebrate evolution.

Online Content Methods, along with any additional Extended Data display items and Source Data, are available in the online version of the paper; references unique to these sections appear only in the online paper.

Received 27 March; accepted 19 May 2017.
Published online 5 July 2017.

1. Grevellec, A. & Tucker, A. S. The pharyngeal pouches and clefts: development, evolution, structure and derivatives. *Semin. Cell Dev. Biol.* **21,** 325–332 (2010).
2. Shone, V. & Graham, A. Endodermal/ectodermal interfaces during pharyngeal segmentation in vertebrates. *J. Anat.* **225,** 479–491 (2014).
3. Dickinson, A. J. G. & Sive, H. Development of the primary mouth in *Xenopus laevis*. *Dev. Biol.* **295,** 700–713 (2006).
4. Soukup, V., Horácek, I. & Cerny, R. Development and evolution of the vertebrate primary mouth. *J. Anat.* **222,** 79–99 (2013).
5. Graham, A. & Richardson, J. Developmental and evolutionary origins of the pharyngeal apparatus. *Evodevo* **3,** 24 (2012).
6. Choe, C. P. & Crump, J. G. Dynamic epithelia of the developing vertebrate face. *Curr. Opin. Genet. Dev.* **32,** 66–72 (2015).
7. Couly, G., Creuzet, S., Bennaceur, S., Vincent, C. & Le Douarin, N. M. Interactions between Hox-negative cephalic neural crest cells and the foregut endoderm in patterning the facial skeleton in the vertebrate head. *Development* **129,** 1061–1073 (2002).
8. Crump, J. G., Swartz, M. E. & Kimmel, C. B. An integrin-dependent role of pouch endoderm in hyoid cartilage development. *PLoS Biol.* **2,** E244 (2004).
9. Piotrowski, T. & Nüsslein-Volhard, C. The endoderm plays an important role in patterning the segmented pharyngeal region in zebrafish (*Danio rerio*). *Dev. Biol.* **225,** 339–356 (2000).
10. Gillis, J. A., Fritzenwanker, J. H. & Lowe, C. J. A stem-deuterostome origin of the vertebrate pharyngeal transcriptional network. *Proc. R. Soc. Lond. B* **279,** 237–246 (2012).
11. Lowe, C. J., Clarke, D. N., Medeiros, D. M., Rokhsar, D. S. & Gerhart, J. The deuterostome context of chordate origins. *Nature* **520,** 456–465 (2015).
12. Kerr, J. G. *The Work of John Samuel Budgett* (Cambridge Univ. Press, 1907).
13. Janvier, P. *Early Vertebrates* (Clarendon, 1996).
14. Quinlan, R., Martin, P. & Graham, A. The role of actin cables in directing the morphogenesis of the pharyngeal pouches. *Development* **131,** 593–599 (2004).
15. Alexander, J. & Stainier, D. Y. A molecular pathway leading to endoderm formation in zebrafish. *Curr. Biol.* **9,** 1147–1157 (1999).
16. Yu, J. K., Holland, L. Z., Jamrich, M., Blitz, I. L. & Holland, N. D. AmphiFoxE4, an amphioxus winged helix/forkhead gene encoding a protein closely related to vertebrate thyroid transcription factor-2: expression during pharyngeal development. *Evol. Dev.* **4,** 9–15 (2002).
17. Suda, Y. *et al.* Evolution of Otx paralogue usages in early patterning of the vertebrate head. *Dev. Biol.* **325,** 282–295 (2009).
18. Rétaux, S. & Pottin, K. A question of homology for chordate adhesive organs. *Commun. Integr. Biol.* **4,** 75–77 (2011).
19. Yoshida, K., Ueno, M., Niwano, T. & Saiga, H. Transcription regulatory mechanism of Pitx in the papilla-forming region in the ascidian, *Halocynthia roretzi*, implies conserved involvement of Otx as the upstream gene in the adhesive organ development of chordates. *Dev. Growth Differ.* **54,** 649–659 (2012).
20. True, J. R. & Haag, E. S. Developmental system drift and flexibility in evolutionary trajectories. *Evol. Dev.* **3,** 109–119 (2001).
21. Soukup, V., Epperlein, H.-H., Horácek, I. & Cerny, R. Dual epithelial origin of vertebrate oral teeth. *Nature* **455,** 795–798 (2008).
22. Cooper, M. S. & Virta, V. C. Evolution of gastrulation in the ray-finned (actinopterygian) fishes. *J. Exp. Zool. B Mol. Dev. Evol.* **308,** 591–608 (2007).
23. Nagasawa, T. *et al.* Evolutionary changes in the developmental origin of hatching gland cells in basal ray-finned fishes. *Zoolog. Sci.* **33,** 272–281 (2016).
24. Satoh, N. *et al.* On a possible evolutionary link of the stomochord of hemichordates to pharyngeal organs of chordates: stomochord and notochord relationship. *Genesis* **52,** 925–934 (2014).
25. Adachi, N. & Kuratani, S. Development of head and trunk mesoderm in the dogfish, *Scyliorhinus torazame*: I. Embryology and morphology of the head cavities and related structures. *Evol. Dev.* **14,** 234–256 (2012).
26. Seifert, R., Jacob, M. & Jacob, H. J. The avian prechordal head region: a morphological study. *J. Anat.* **183,** 75–89 (1993).
27. Oisi, Y., Ota, K. G., Kuraku, S., Fujimoto, S. & Kuratani, S. Craniofacial development of hagfishes and the evolution of vertebrates. *Nature* **493,** 175–180 (2013).
28. Sessel, A. in *Archiv für Anatomie und Entwickelungsgeschichte* (Veit & Comp., 1877).
29. Godard, B. G. *et al.* Mechanisms of endoderm formation in a cartilaginous fish reveal ancestral and homoplastic traits in jawed vertebrates. *Biol. Open* **3,** 1098–1107 (2014).
30. Takeuchi, M., Takahashi, M., Okabe, M. & Aizawa, S. Germ layer patterning in bichir and lamprey; an insight into its evolution in vertebrates. *Dev. Biol.* **332,** 90–102 (2009).
31. Hatschek, B. & Tuckey, J. *The Amphioxus and its Development* (Swan, Sonnenschein & Co., 1893).

Supplementary Information is available in the online version of the paper.

Acknowledgements We thank C. V. H. Baker, M. E. Bronner, M. M. Smith, A. S. Tucker, D. M. Medeiros, P. E. Ahlberg, and S. Kuratani and his laboratory members for their helpful comments; and I. Čepička, whose laboratory members initially assisted with the gene cloning procedures. V. Miller and K. Kodejš are acknowledged for their care of bichirs in Prague, and M. Kahanec and M. Rodina for their care of sturgeons in Vodňany. D.J. thanks C. V. H. Baker for hosting him in her laboratory and the European Molecular Biology Organization (EMBO) for financial support. The study was supported by GACR project 16-23836S (R.C.); Charles University grant SVV 260 434 / 2017 and Charles University GA UK projects 220213 and 726516 (M.M.), and 1448514 (J.S.). M.M. thanks the OeAD Aktion Österreich-Tschechien scholarship (financed by BMWFW Austria) for financial support during his stay in B.D.M.'s laboratory. M.P. and D.G. thank the Ministry of Education, Youth and Sports of the Czech Republic (projects CENAKVA (CZ.1.05/2.1.00/01.0024), CENAKVA II (LO1205 under the NPU I program)). L.A.R. thanks the SAGARPA-COFUPRO (RGAC-GTOS-2011-027): "Equipamiento para el Fortalecimiento del Núcleo Genético de pejelagarto en el estado de Tabasco".

Author Contributions R.C. and M.M. conceived the project; M.M. performed most experiments; J.S., P.F. and D.J. performed gene cloning and some experiments; D.J. performed phylogenetic analyses; B.D.M. and M.M. performed micro-CT analyses; M.P. and D.G. provided sturgeon embryonic material; L.A.R. provided gar embryonic material and A.O.P. assisted with gar and sturgeon experiments; R.C., M.M. and I.H. wrote the manuscript with input from all authors.

Author Information Reprints and permissions information is available at www.nature.com/reprints. The authors declare no competing financial interests. Readers are welcome to comment on the online version of the paper. Publisher's note: Springer Nature remains neutral with regard to jurisdictional claims in published maps and institutional affiliations. Correspondence and requests for materials should be addressed to R.C. (robert.cerny@natur.cuni.cz).

Reviewer Information *Nature* thanks A. Gillis, G. Schlosser and the other anonymous reviewer(s) for their contribution to the peer review of this work.

METHODS

Embryos. All experiments were in full compliance with guidelines for the use of embryonic material and were approved by the institutional animal care and use committee of the Charles University in Prague, Czech Republic, where this work took place. All experimental procedures used in sturgeons were approved by the Animal Research Committee of Faculty of Fisheries and Protection of Waters in Vodnany, Czech Republic. Fish sampling and experimental work in Mexico followed the authorization and regulations of the Mexican Federal Agency CONAPESCA.DGOPA.09004.041111.3088 and the ethical and research regulations of the Universidad Juárez Autónoma de Tabasco, México.

Adult bichirs were kept in aquaria at the Department of Zoology, Charles University in Prague, and their spawning was stimulated naturally by water and temperature conditions during the breeding season from October to April. Fertilized eggs were collected from the breeding tanks and transferred to a separate beaker and kept at 28 °C. Adult sturgeons were bred in the hatcheries of the Research Institute of Fish Culture and Hydrobiology in Vodnany, University of South Bohemia in Ceske Budejovice. Fertilized eggs were shipped in water-filled plastic bags directly to the laboratory at the Department of Zoology, Charles University in Prague. Live embryos at the blastula stage were transferred to well-oxygenated tanks and incubated at 17 °C in E2 Pen/Strep zebrafish embryo medium[32]. At appropriate stages, specimens were collected for experiments and further analyses. Gars were bred at the División Académica de Ciencias Biológicas, Universidad Juárez Autónoma de Tabasco in Villahermosa, Tabasco, Mexico. After artificial spawning, the eggs were transferred to plastic containers and kept at 28 °C until they reached the desired stage.

All embryos for fate-mapping experiments were randomly selected, decapsulated and kept in E2 Pen/Strep medium on Petri dishes with agar. For histological analyses and immunohistochemistry embryos were anaesthetized in MS-222 (Serva), fixed in 4% PFA and stored at 4 °C. Embryos for SEM were decapsulated and postfixed in Karnovsky's fixative (2% glutaraldehyde in 4% PFA) for at least 24 h. Specimens for *in situ* hybridization (ISH) were fixed in 4% PFA overnight and stored in 100% methanol at −20 °C until further processed.

Micro-CT imaging and data analysis. PFA-fixed embryos were postfixed in Karnovsky fixative at least overnight and then kept in 70% EtOH. To introduce high differential contrast to the soft tissues, samples were treated with 1% phosphotungstic acid (PTA)[33] in 70% EtOH overnight. Subsequently, samples were mounted in 2.5% agar into 200-µl pipette tips, attached to a sample holder and scanned using MicroXCT (Xradia) at the Department of Theoretical Biology, University of Vienna, Austria. The reconstructed virtual sections were analysed in Amira (FEI software). To visualize the extent of embryonic head endoderm, endodermal tissue was manually segmented based on relatively high contrast of the yolk granules, and visualized in yellow as a surface rendering within the context of the whole embryo. The entire embryos were visualized either by volume rendering or maximum intensity projection, as indicated in the figures.

Scanning electron microscopy. Specimens for SEM were fixed in PFA at least overnight and then postfixed overnight in Karnovsky's fixative. After a PBS wash they were dehydrated in ethanol and dried in a critical point dryer (Baltec CPD 030). Dry samples were mounted on resin-covered tungsten discs and coated with gold using sputter coater (Baltec SCD 050). SEM imaging was performed on a JEOL 6380 LV scanning electron microscope.

Fate-mapping. Neurula stage embryos of bichirs (stages 18–19 (ref. 34), Extended Data Fig. 1), sturgeons (stages 21–22 (ref. 35), Extended Data Fig. 2) and gars (stages 15–16 (ref. 36), Extended Data Fig. 3) were manually decapsulated and mounted into agar chambers in E2 Pen/Strep medium before injection. CM-DiI cell tracking dye (Thermo Fisher Scientific) stock solution (10 µg in 50 µl 100% EtOH) was diluted to working concentration (1:5) with 10% sucrose and kept in an ultrasonic cleaner to prevent dye precipitation. Fifty-microlitre capillaries (Drummond Microcaps) were pulled using Narishige pc-10 puller and the tips broken at the appropriate diameter. A manual microinjector (Eppendorf CellTram vario) was used to inject the cell tracker. To avoid staining of ectoderm and mesoderm, the capillary was aimed from above through the anterior neural plate. The dye was released slowly to prevent rupture of epithelia, aiming from back to front to preferentially stain the anterior foregut wall and future pharynx (Fig. 3a). Excess dye leaking from the injection wound was gently removed by a flow of liquid and embryos were moved to fresh medium. As a control, embryos were fixed immediately in PFA, sectioned medially in an agarose block and observed under fluorescent stereomicroscope (Zeiss Lumar.V12), in order to confirm proper location of the dye (Fig. 3b). The remaining specimens were incubated in E2 Pen/Strep medium until they reached the desired stage. This experimental setup resulted in embryos with CM-DiI-stained endodermal epithelia, while the ectoderm-derived tissues remained unstained, except for the original injection site at the dorsal head surface (Fig. 3b, c).

The sample size per species was based on its reproductive biology and general accessibility of the material and was not predetermined by statistical methods. In the case of bichir, 26 embryos from the 2011, 2013, and 2017 seasons were successfully injected (that is, they did not show any unintentional staining in neural crest or head mesoderm-derived tissues due to inappropriate aiming of the injection capillary). All of these embryos showed positive staining in the inner endodermal derivatives such as pharyngeal pouches, oral endoderm, and yolk and ten specimens showed positive staining in the pre-oral gut-derived cement gland cells (Fig. 3g,h). In the case of sturgeons, 117 embryos were successfully injected and fixed in stages 36 ($n = 35$), 38 ($n = 24$), 40 ($n = 16$) and 45 ($n = 42$) during the 2015 and 2016 seasons. Among these, 79 specimens showed positive signal in pre-oral endodermal derivatives located at the facial surface (20 in stage 36; 14 in stage 38; 12 in stage 40; and 33 in stage 45) (Extended Data Fig. 8). In the case of gars, 167 embryos were successfully injected during the 2014, 2015, and 2016 seasons, and 155 of these showed positive CM-DiI staining in the cement gland, as well as in other endodermal derivatives of the pharynx (4 in stage 16, 106 in stages 23–24, 45 in stages 25–28) (Extended Data Fig. 10). Given the descriptive nature of the imaging analyses of the injected embryos, the investigators weren't subject to blinding for group allocations for the aim of the fate-mapping experiment.

Histological and immunohistochemical staining. To better reveal tissue context in the analysed specimens, basal laminae were stained on sections using anti-fibronectin antibody (Dako A0245, 1/500). To visualize actin fibres, anti-actin (Sigma-Aldrich A1978, 1/1,000) antibody was used. The primary antibodies were then detected via fluorescent secondary antibodies or with an avidin-biotin Vectastain kit (Vector). Nerve fibres were detected using anti-acetylated tubulin antibody (Sigma-Aldrich T6793, 1/2,000) and EnzMet Enzyme Metallography kit (Nanoprobes) on whole-mount embryos. Sections were mounted with DAPI-containing Fluoroshield histology mounting medium (Sigma-Aldrich) and photographed using a fluorescent microscope (Olympus BX51). PAS staining was performed using a PAS kit (Sigma) according to the manufacturer's instructions. Prior to wholemount staining, the embryos were treated with sodium bisulfite (1,041 g in 100 ml distilled water) for 4 h at room temperature. Stained wholemount specimens were photographed under an Olympus SZX12 stereomicroscope.

Gene cloning and *in situ* hybridization. The riboprobes used in this study were synthesized from *P. senegalus*, *A. ruthenus*, and *A. tropicus* cDNA using the following primer sequences: *P. senegalus Pitx2*: 5′-CCAGYCCNGAGKCYAGAGAAAG-3′ and 5′-GCRCTSAGRTTKGABSCBGGRTTCTG-3′; *A. ruthenus Sox17*: 5′-TTTAGGTGACACTATAGCCTGCATGTGCTGCACTCTA-3′ and 5′-GGACACTGTCAGTGGACAGA-3′, *FoxE4*: 5′-CCHGGSAARGGMAAYTACTGGAC-3′ and 5′-TSAYDGRCTGRGWCTGRAAACA-3′, *Pitx2:* 5′-ATTTAGGTGACACTATAGTGGAGTTGCAAGTGTCCCTA-3′ and 5′-ATGCAGCCCTACGAAGACAT-3′, *Otx2:* 5′-ATTTAGGTGACACTATAGTAATCCAAGCAGTCGGAAGTGGGGT-3′ and 5′-TCCACCCCGGCCATCCCCAG-3′; *A. tropicus Sox17*: 5′-ATTTAGGTGACACTATAGCGAGGCCGGTATTTGTAGTT-3′ and 5′-TCTACCACCCTTTGGAAGCC-3′, *FoxE4*: 5′-TCHCCSACYGARGCYKCCAG-3′ and 5′-ATRCTRAACATSCKRTGYTG-3′, *Pitx2*: 5′-CGTATTGGCAAGCACTCAGA-3′ and 5′-CCAATCTCACAGAAGCACGA-3′, *Otx2*: 5′-ATTTAGGTGACACTATAGCAGTCTGCCGCCGAGTTGAA-3′ and 5′-GCAGCAACAGCAGCAGCAGA-3′. The PCR fragments were T/A cloned using pGEM-T-Easy Vector Systems (Promega) following the manufacturer's instructions. Orthology was checked by reconstructing phylogenetic relationships (Supplementary Table 1). Obtained sequences were deposited in GenBank (Supplementary Table 1).

Methanol-fixed embryos were rehydrated, depigmented in a bleaching solution (Formamide, 20× SSC, hydrogen peroxide and distilled water) and digested by 2 µg/ml Proteinase K (Sigma-Aldrich). Digested embryos were PFA-postfixed for 20 min and subsequently transferred into hybridization solution (50% formamide, 4× SSC, 0.1 mg/ml heparin, 1× Denhardt's, 0.1% CHAPS, 0.2 mg/ml yeast RNA, 10 mM EDTA, 0,1% Tween-20) and after several changes incubated in hybridization solution with digoxigenin (DIG)-labelled RNA probes (1:1,000, overnight at 60 °C). After incubation, the embryos were washed several times in post-hybridization solution (50% formamide, 4× SSC, 0.1% Tween-20) and transferred via MABT (100 mM maleic acid, 150 mM NaCl, 0.1% Tween-20) into blocking solution (2% blocking reagent, 20% sheep serum). Embryos were incubated with alkaline phosphatase-conjugated antibody against DIG (Roche, 1:3,000) at 4 °C overnight, washed several times in MABT, then put into NTMT (0.1 M Tris, 0.1 M NaCl, 0.05 M $MgCl_2$) and kept in BM Purple substrate (Roche) at 4 °C until signal developed.

Imaging and sectioning. The CM-DiI injected specimens were anaesthetized in MS-222 (Serva) and fixed in 4% PFA for further analysis. For whole-mount imaging the specimens were washed in PBS, mounted into agar chambers and photographed using a fluorescent stereomicroscope (Zeiss Lumar.V12). Sturgeon

and gar specimens were then embedded in agar, or in gelatine/albumin solution, and sectioned on a vibratome (Leica VT1200S) with section thickness set to 40 μm. Bichir embryos were embedded in 20% gelatin and sectioned using a cryomicrotome (Leica CM3050S) to 8 μm section thickness. Specimens for ISH were photographed under a stereomicroscope (Olympus SZX12) and subsequently sectioned on a vibratome as described above, and mounted with DAPI-containing Fluoroshield histology mounting medium (Sigma-Aldrich) to better visualize tissue context. DAPI signal was converted to red channel and then inverted in FIJI to show cyan nuclei on a white background to allow merging with the bright field image of the vibratome section. Embryos for resin histology were dehydrated in ethanol and embedded in JB-4 (Polysciences) according to the manufacturer's instructions. Embryos in solid resin blocks were sectioned on a microtome (Leica RM2155), stained with Azure B/Eosin (Serva) and mounted in DPX (Fluka).

Data availability. Obtained sequences were deposited in GenBank (Supplementary Table 1). All other data are available from the corresponding author upon reasonable request.

32. Brand, M., Granato, M. & Nüsslein-Volhard, C. in *Zebrafish* (Oxford Univ. Press, 2002).
33. Metscher, B. D. MicroCT for comparative morphology: simple staining methods allow high-contrast 3D imaging of diverse non-mineralized animal tissues. *BMC Physiol.* **9,** 11 (2009).
34. Diedhiou, S. & Bartsch, P. in *Development of Non-Teleost Fishes* (Science Publishers, 2009).
35. Dettlaff, T. A., Ginsburg, A. S. & Schmalhausen, O. I. *Sturgeon Fishes—Developmental Biology and Aquaculture* (Springer, 1993).
36. Long, W. L. & Ballard, W. W. Normal embryonic stages of the longnose gar, *Lepisosteus osseus*. *BMC Dev. Biol.* **1,** 6 (2001).

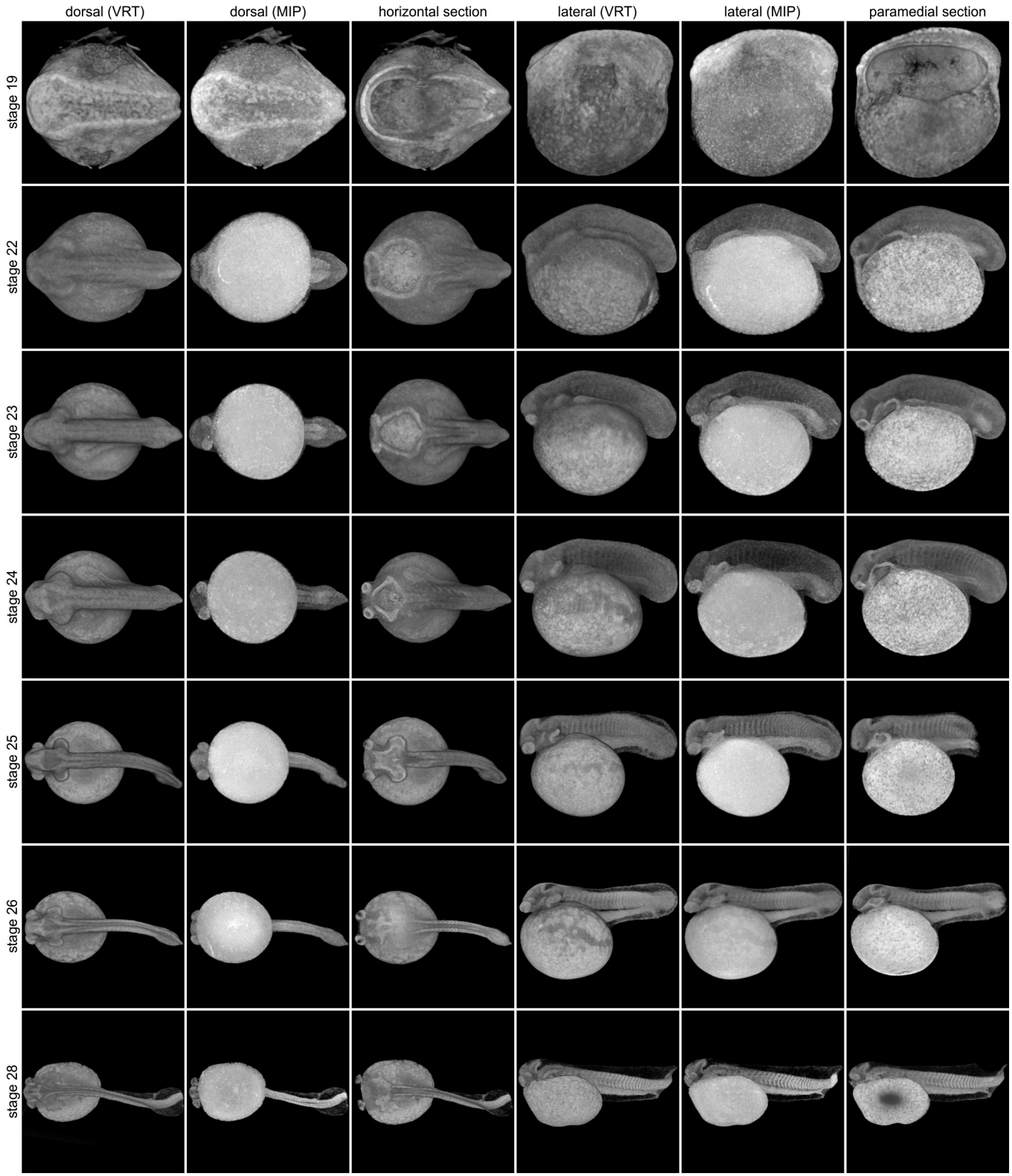

Extended Data Figure 1 | Micro-CT visualization of bichir embryogenesis. Stages 19–28 (ref. 34).

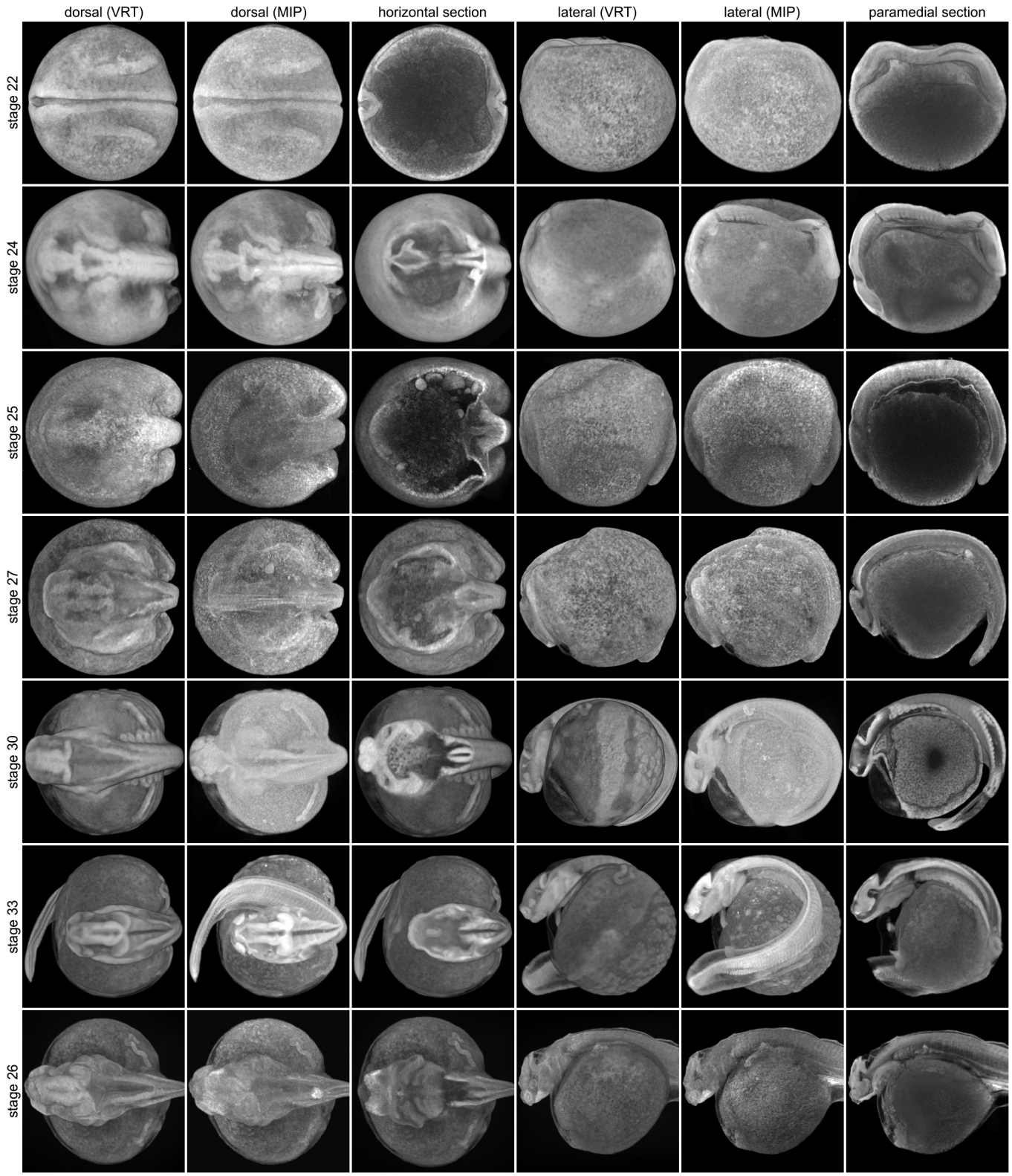

Extended Data Figure 2 | Micro-CT visualization of sturgeon embryogenesis. Stages 22–26 (ref. 35).

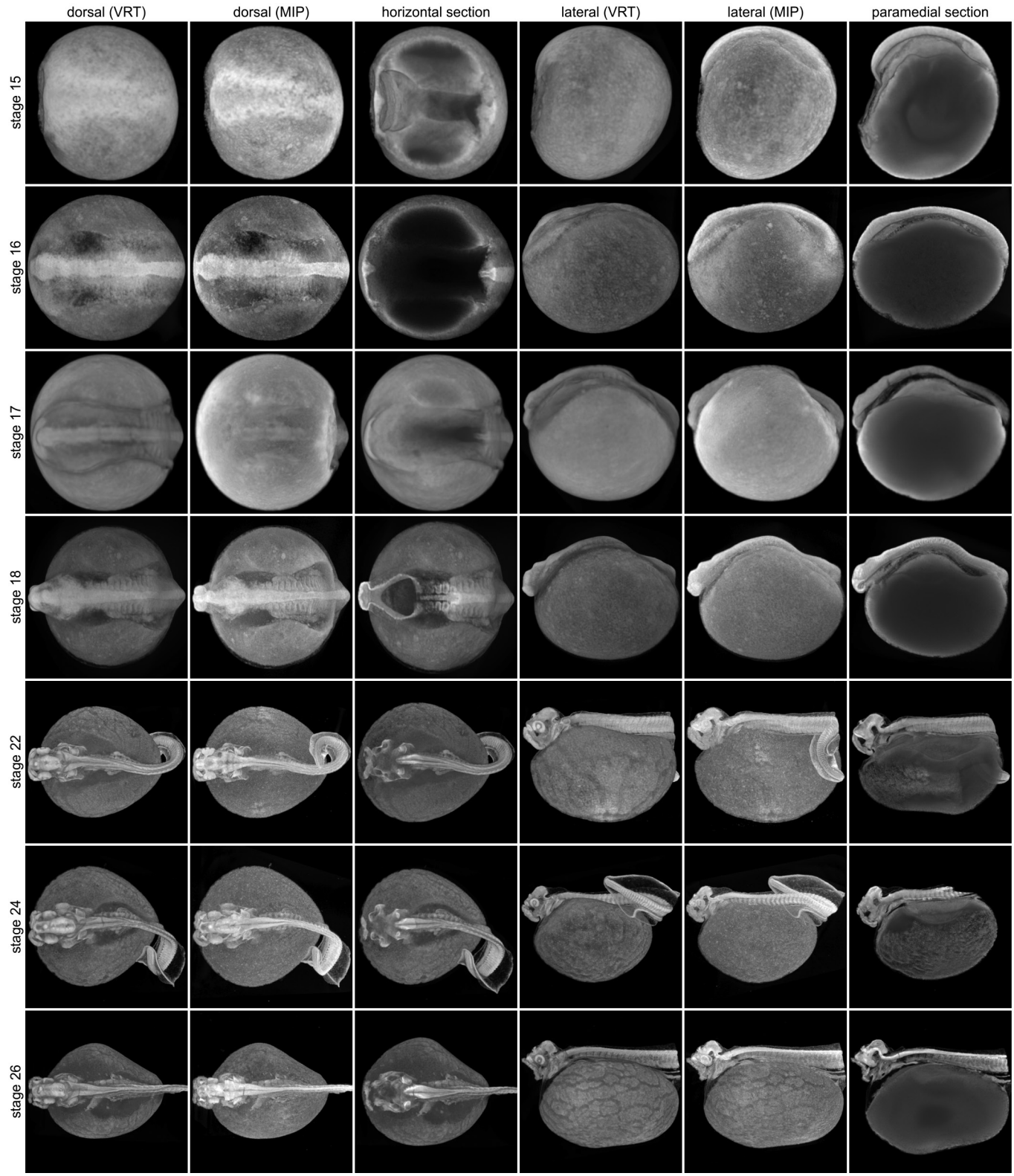

Extended Data Figure 3 | Micro-CT visualization of gar embryogenesis. Stages 15–26 (ref. 36).

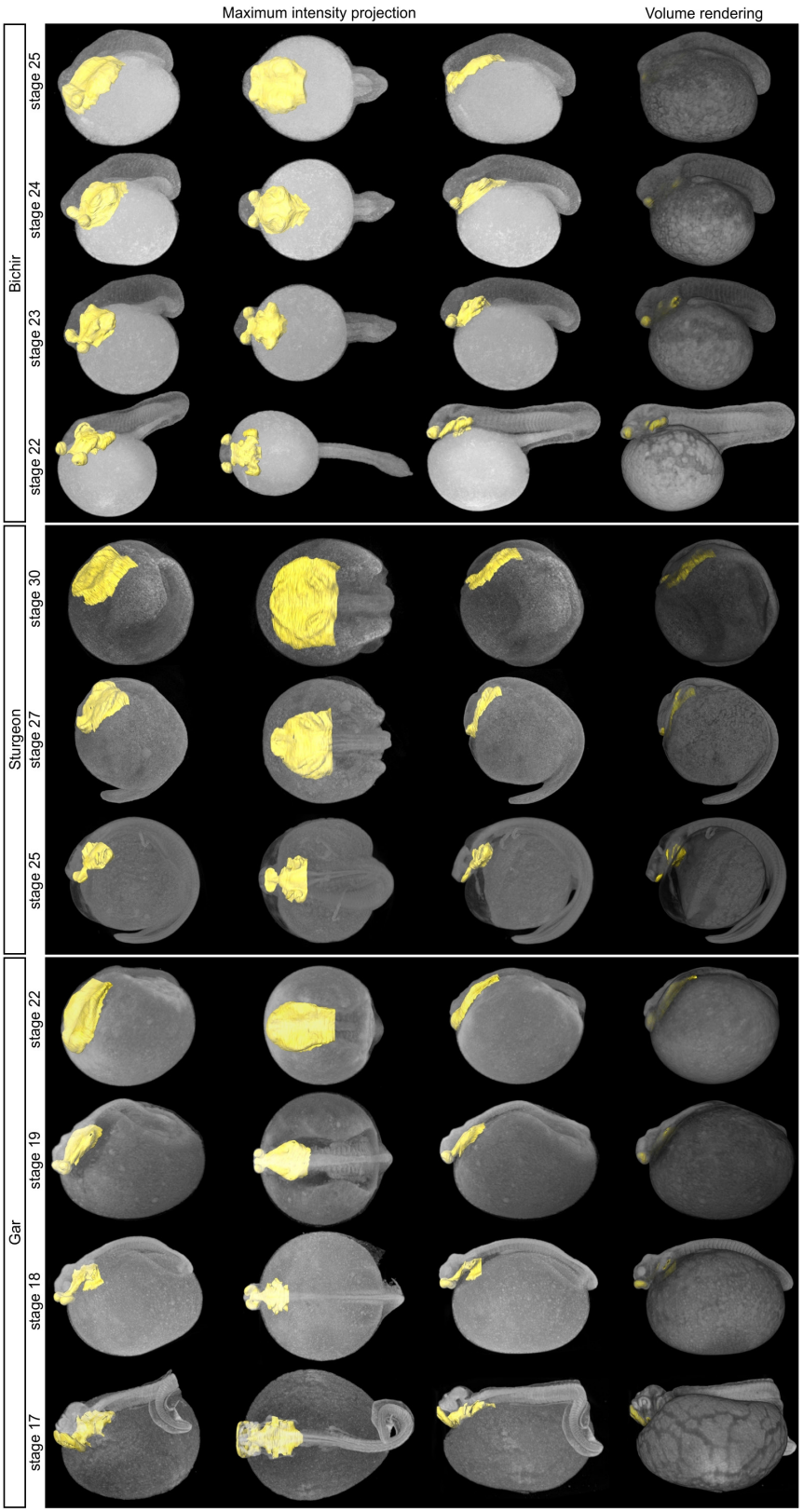

Extended Data Figure 4 | Micro-CT visualization of pharyngeal development (yellow) in bichir, sturgeon and gar. 3D reconstructions of key developmental stages.

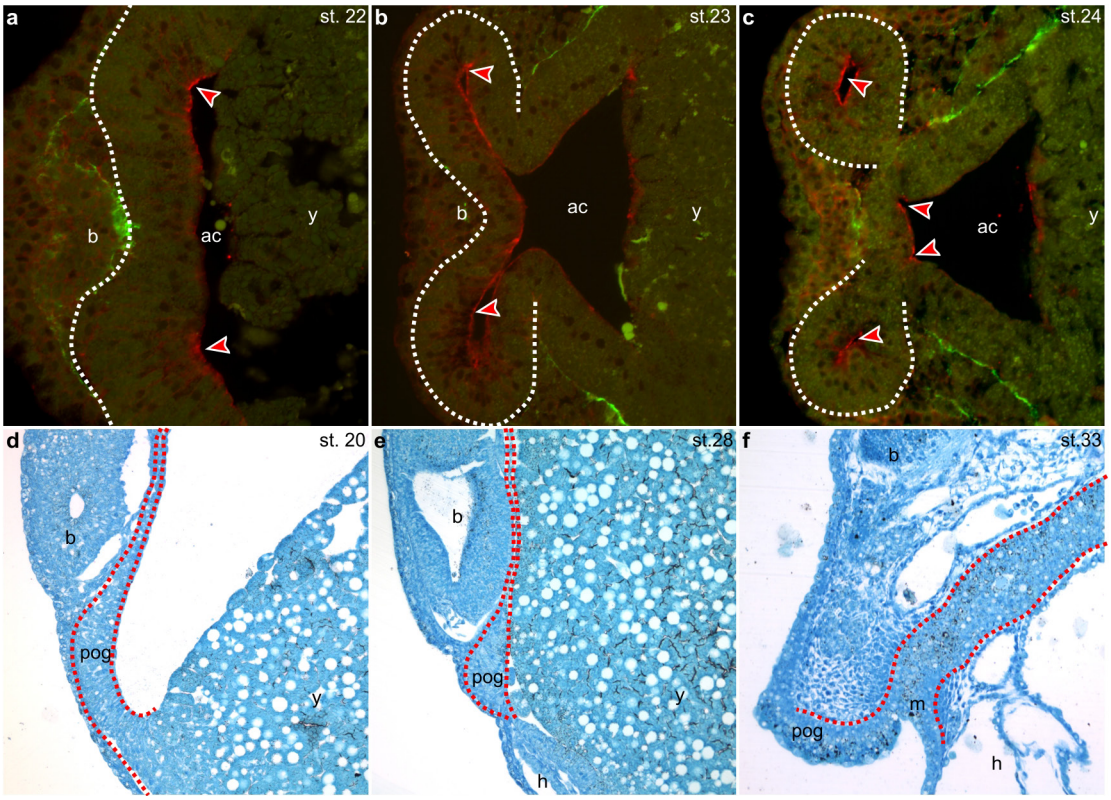

Extended Data Figure 5 | Outpocketing of POGD in bichir and secondary constriction of POGD in sturgeon pharyngulae during development. a–c, Horizontal vibratome sections of bichir pharyngulae at three succeeding stages, showing formation of POGD and cement glands. Head to the left; white dotted line delineates POGD. Fibronectin (green) marks cell and tissue borders; actin (red) stains contracting actin fibres during POGD formation. Red arrowheads point to the possible role of actin cables in POGD outpocketing. **d–f**, Plastic parasagittal sections of sturgeon pharyngulae at three succeeding stages. Head to the left; stained with AzureB/eosin. Red dotted line delineates POGD. b, brain; h, heart; pog, pre-oral gut.

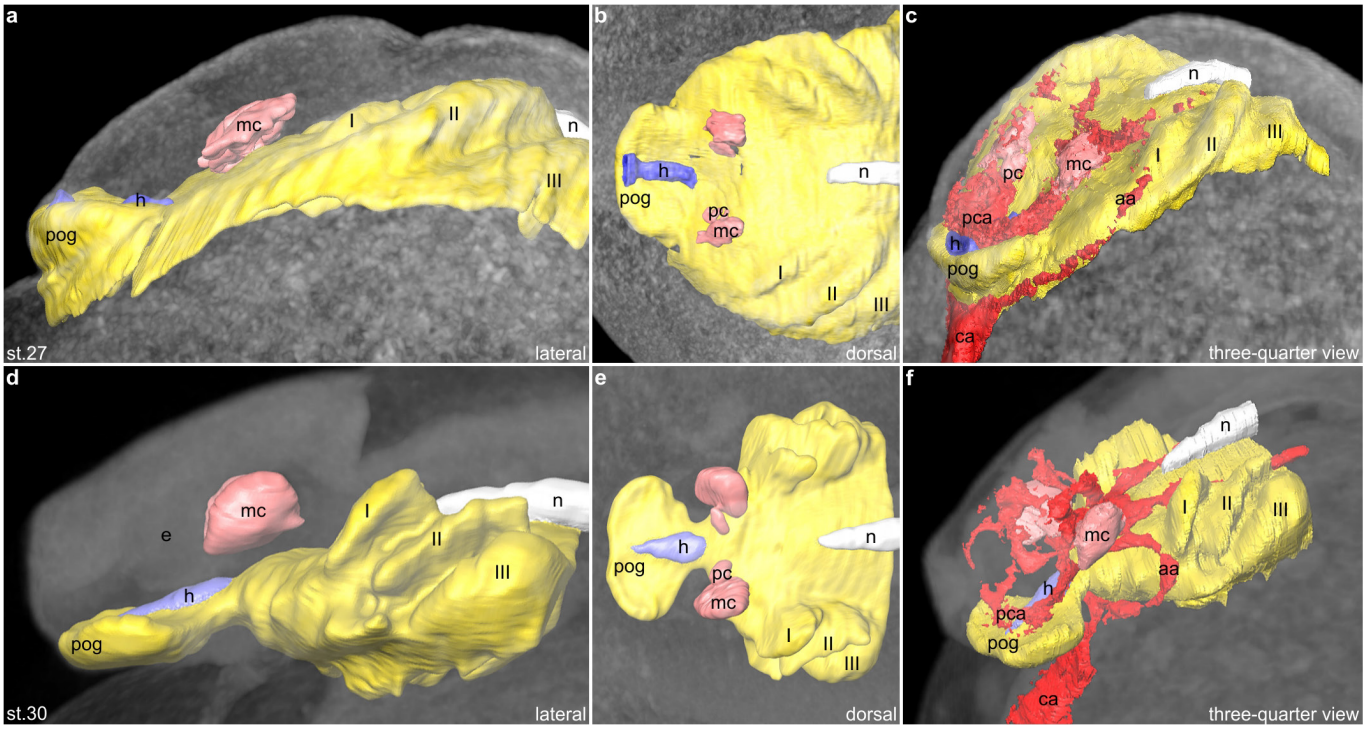

Extended Data Figure 6 | Micro-CT visualization of sturgeon pharynx at two key developmental stages. 3D reconstructions showing the position of pre-oral gut (pog), adenohypophysis (blue), notochord (white), and condensations of head mesenchyme (pink). Endoderm is yellow; roman numerals refer to pharyngeal pouches; red colour shows cranial arteries. aa, aortic arches; h, adenohypophysis; mc, mandibular head cavity.

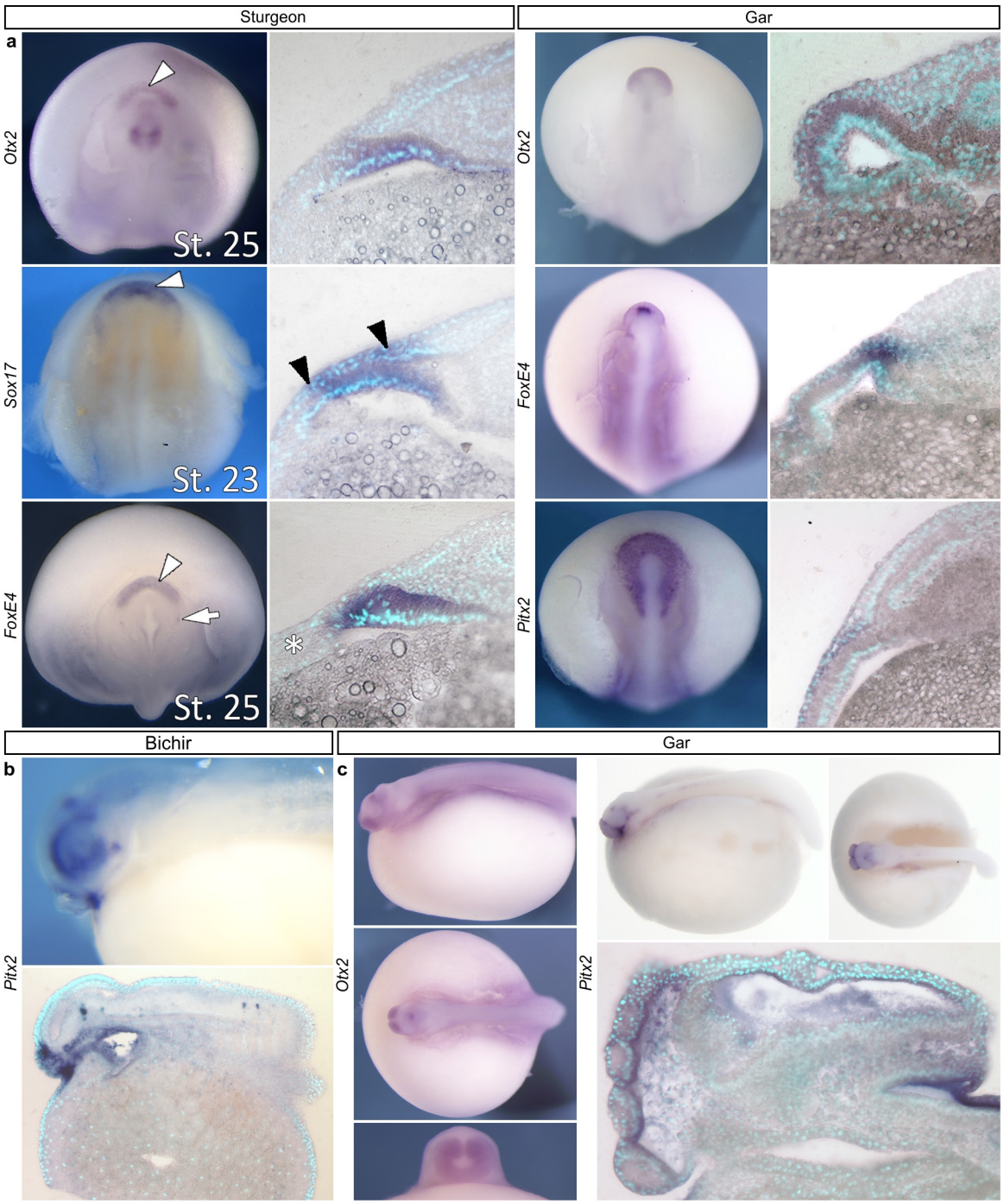

Extended Data Figure 7 | Gene expression patterns (*Otx2*, *Sox17*, *FoxE4* and *Pitx2*) in POGD in bichir, sturgeon and gar embryos. Wholemount views and parasagittal vibratome sections (head to the left); DAPI (blue) stains cell nuclei.

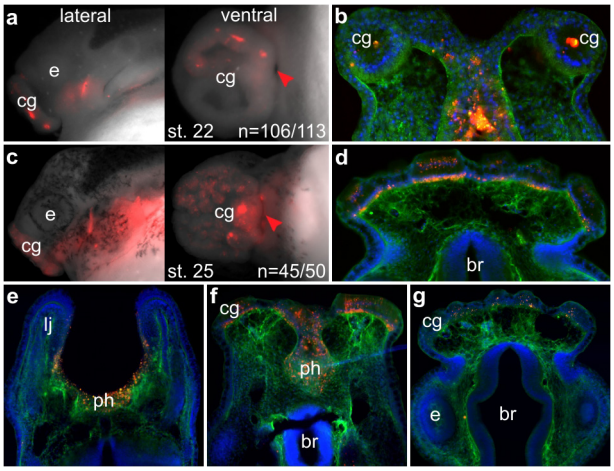

Extended Data Figure 8 | CM-DiI fate-mapping of the primitive gut in gars, with endodermal contribution to the orofacial surface. **a**, **c**, Experimental gar embryos, wholemount lateral and ventral view, respectively, with CM-DiI (red) in pharynx and cement glands. Red arrowhead indicates mouth. **b**, **d**–**g**, Horizontal sections, anterior head with CM-DiI (red) in forming cement glands and cranial surface. DAPI (blue) stains cell nuclei; fibronectin (green) marks cell and tissue borders.

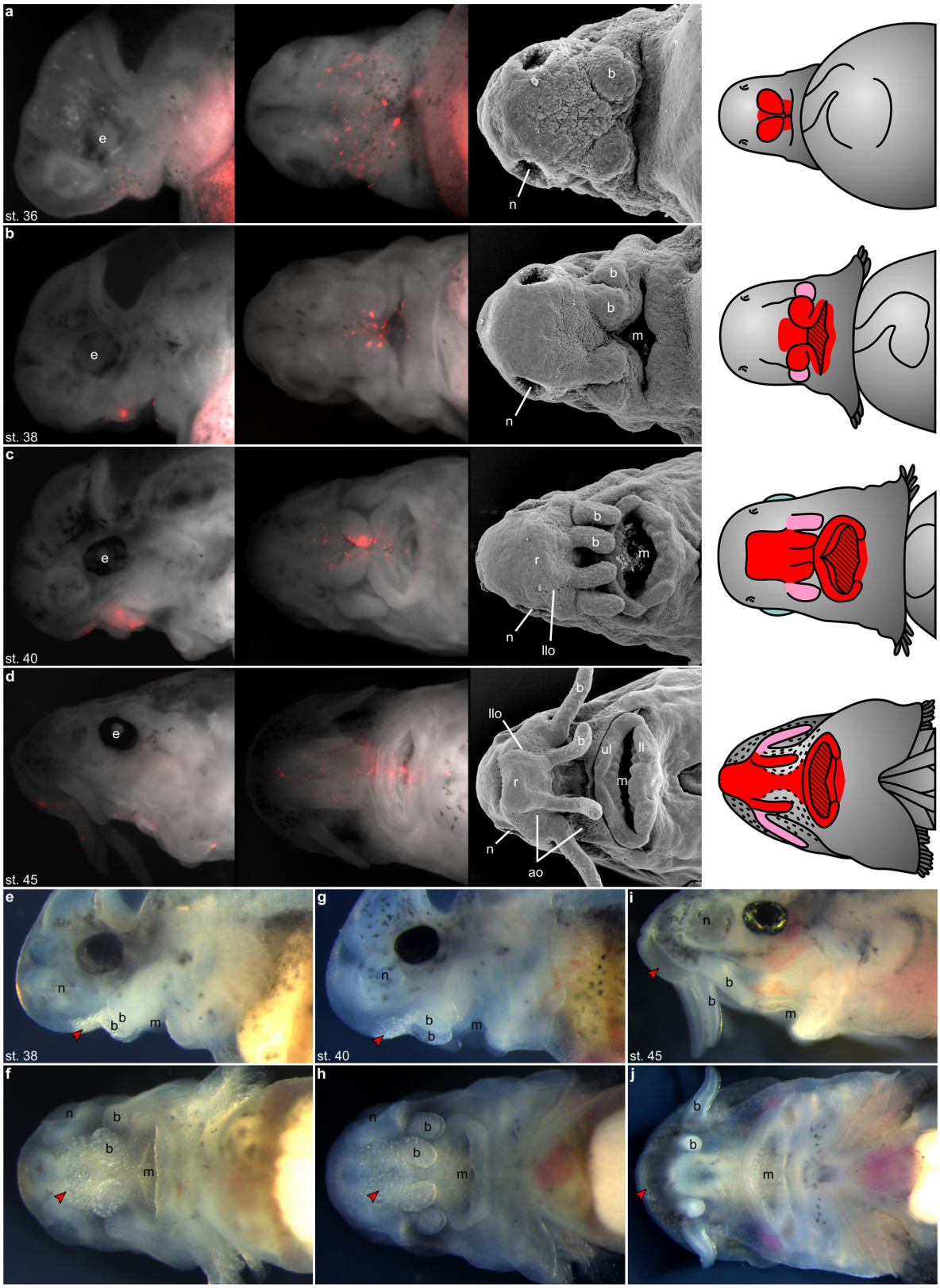

Extended Data Figure 9 | CM-DiI fate-mapping of the primitive gut in sturgeons, with endodermal contribution to the orofacial surface. **a**–**d**, Experimental sturgeon embryos showing the extent of CM-DiI (red) at stages just before (**a**), during (**b**), and after (**c**, **d**) mouth opens. Left to right show lateral views, ventral views, SEM images, and schematics. **e**–**j**, Sturgeon embryos; bright field images, showing the presence and extent (red arrows) of the yolk-rich cells of the foregut endoderm. These cells appear full of bright yolk granules, which gradually disappear during later development (**i**, **j**).

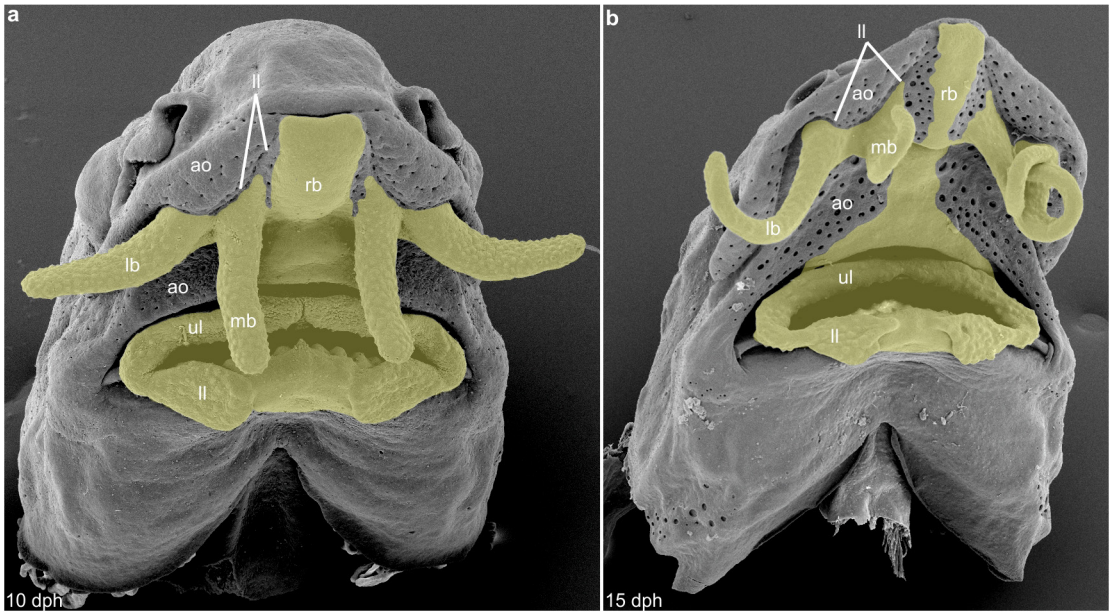

Extended Data Figure 10 | SEM images of sturgeon head mapping experimental fate-mapping data with endodermal contribution pseudocoloured yellow. Antero-ventral views, 10 and 15 days post hatching (d.p.h.); mb, medial barbel; lb, lateral barbel; ao, ampullary organs; rb, rostrum.